Supporting Information

Enhanced broadband fluorescence detection of nucleic acids using multipolar gap-plasmons on biomimetic Au metasurfaces

*Vinayak Narasimhan,[a] Radwanul Hasan Siddique,[a] Magnus Hoffmann,[b] Shailabh Kumar[a] and Hyuck Choo[a]**

[a] Department of Medical Engineering, California Institute of Technology, Pasadena, CA 91125, USA
[b] Department of Biology and Biological Engineering, California Institute of Technology, Pasadena, CA 91125, USA
* E-mail: hyuck.choo@samsung.com; hchoo@caltech.edu

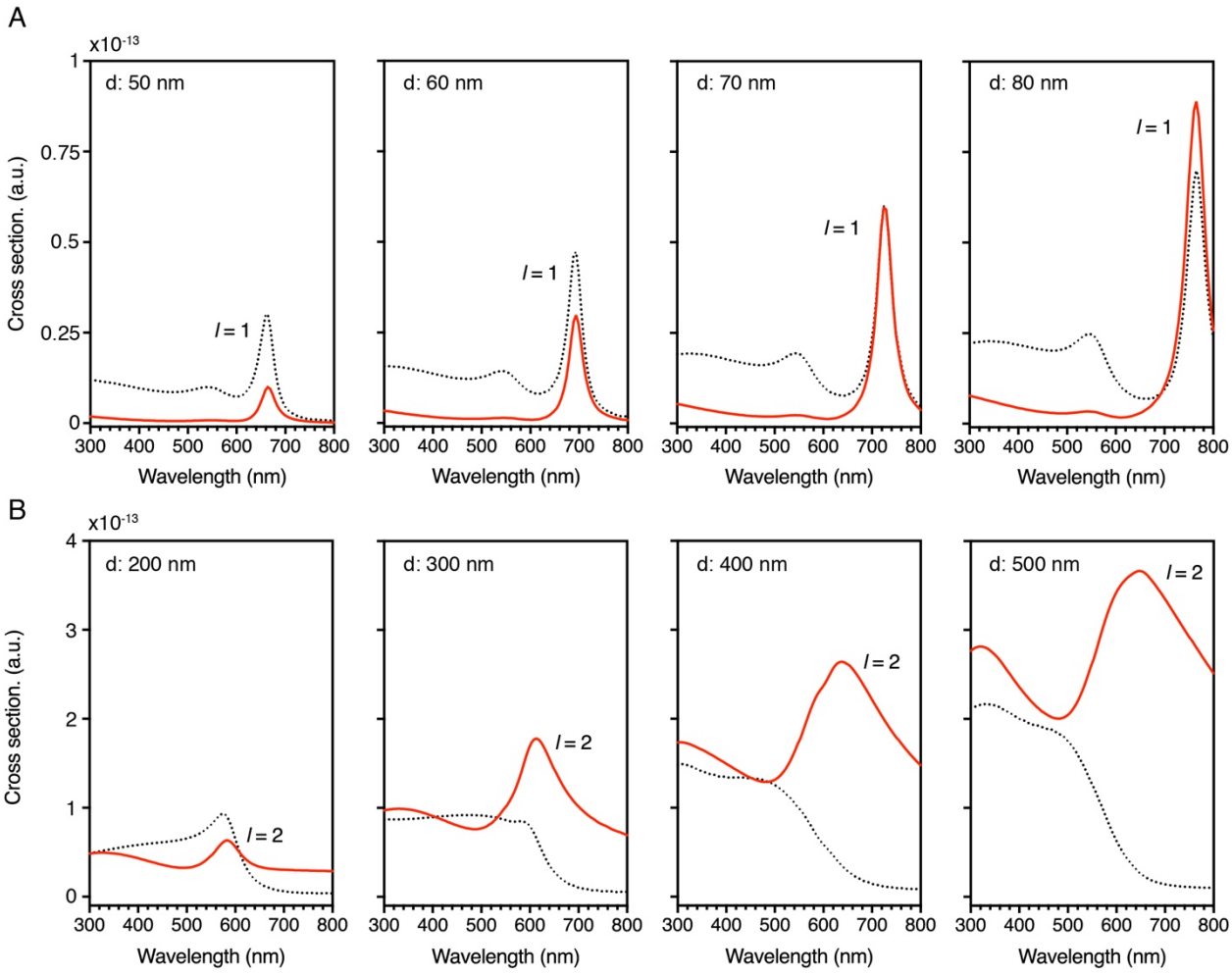

Fig. S1 The absorption (dotted black) and scattering (solid red) cross sections in the Vis-NIR regime of (a) the $l = 1$ dipolar mode of smaller MIM structures with diameters from 50 – 80 nm and (b) the $l = 2$ quadrupolar mode of larger MIM structures with diameters from 200 – 500 nm. The ratio of the scattering to absorption cross section is considerably higher for the $l = 2$ mode compared to the $l = 1$ mode.

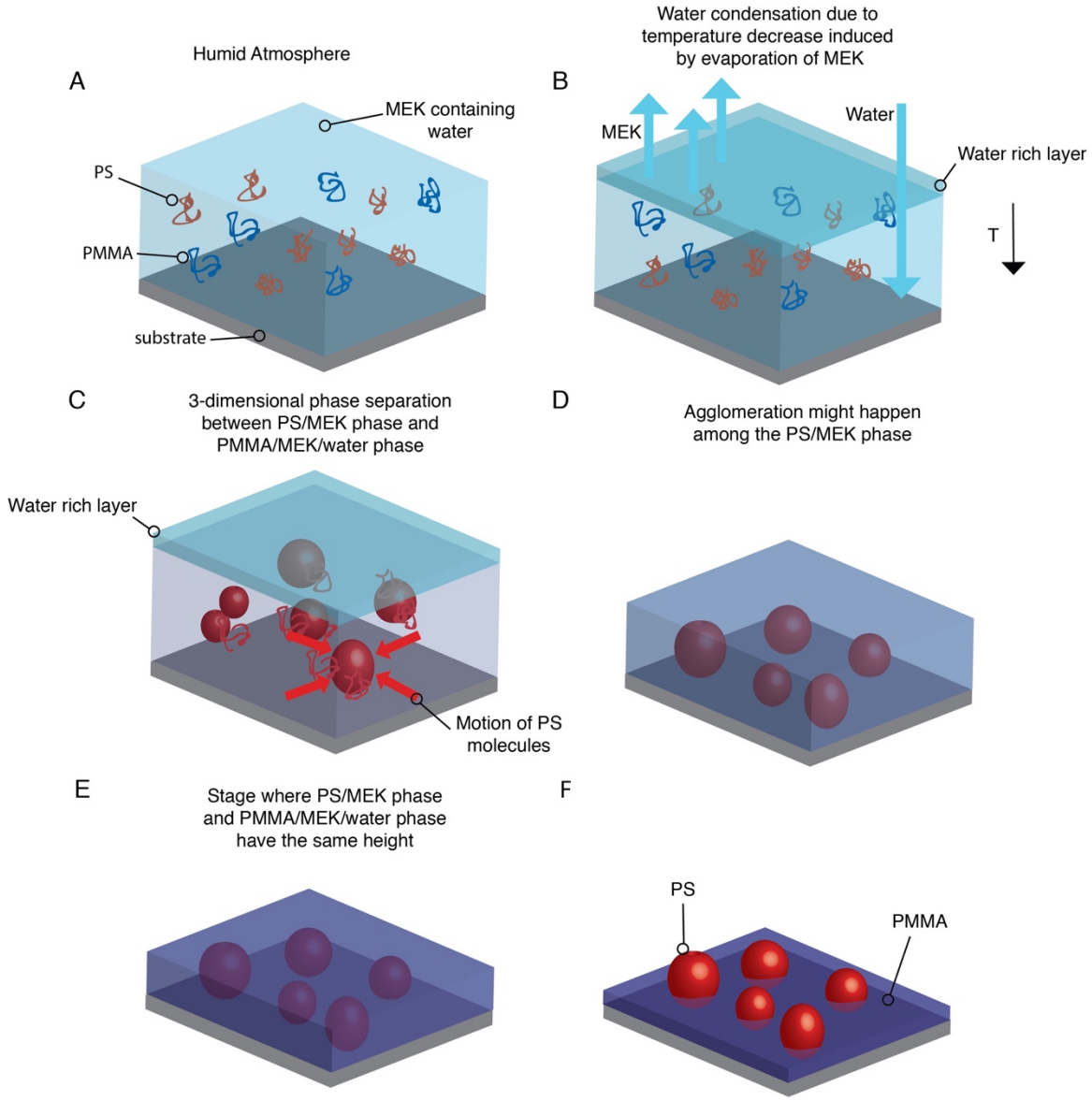

Fig. S2. Schematic illustrations of different phases of the 3-dimensional phase separation process of the self-assembly technique (adapted from[1]).

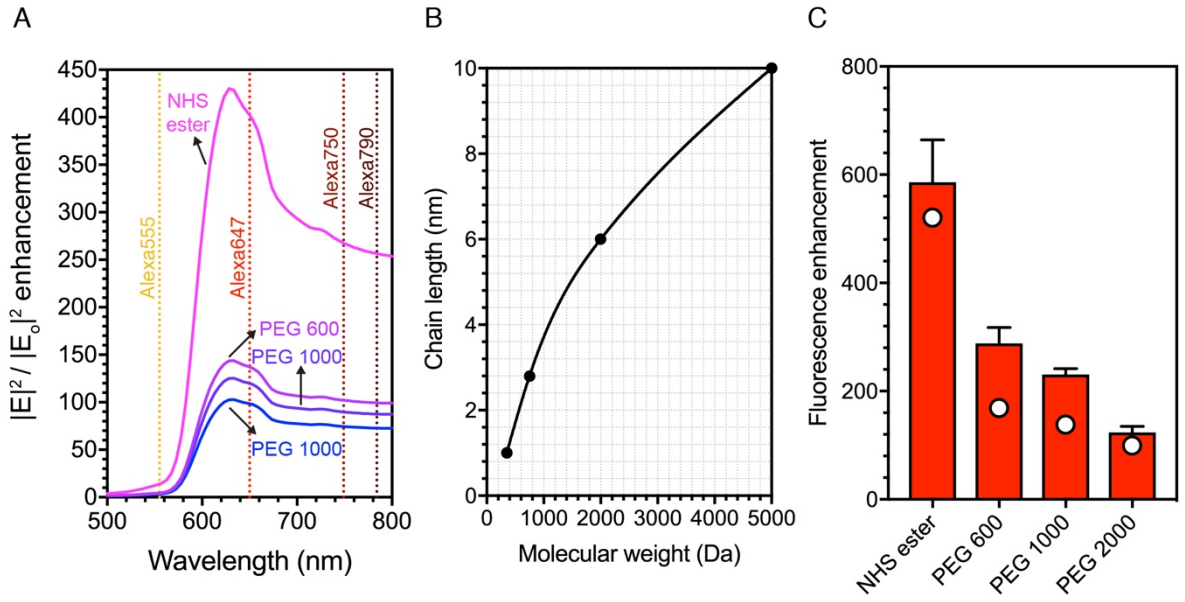

Fig. S3. (a) Normalized $|E|^2$ enhancement computed through FDTD experienced by emitters at various distances from the plasmonic hotspot of an MIM structure of diameter 340 nm. The diameter corresponds to the mean diameter of the samples used the work. Dotted lines correspond to the excitation maxima of each fluorophore used in the study. NHS ester corresponds to a distance of ~ 0 nm while (b) PEG 600, PEG 1000 and PEG 2000 correspond to distances of ~ 0, 7, 8.75 and 11 nm respectively.[2] (c) Fluorescence enhancement factor of Alexa Fluor 647 at various distances from the plasmonic hotspot of the MIM-MS. Numerically computed enhancement factors for the same distances are plotted as dots.

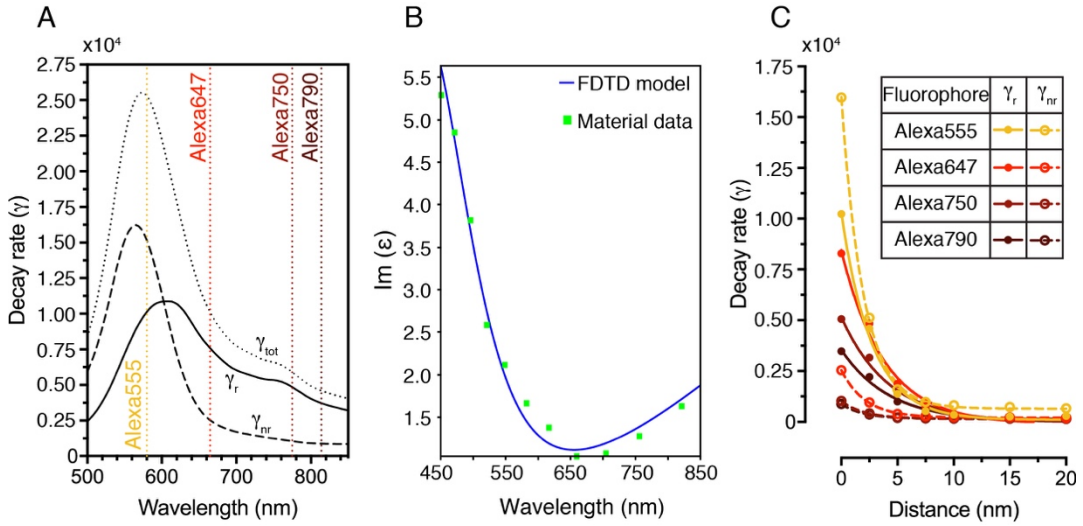

Fig. S4. (a) The radiative (γ_r, solid), nonradiative (γ_{nr}, dashed) and total (γ_{tot}, dotted) decay rates versus wavelength at an emitter distance of 0 nm from an MIM structure of diameter 340 nm computed through FDTD. The vertical dotted lines correspond to the emission maxima of the fluorophores used in the study. The peak position of γ_r correlates well with the plasmon resonance wavelength of the $l = 2$ mode of the structure. (b) High absorption for wavelengths less than 500 nm which corresponds to losses through nonradiative channels is due to high intrinsic material losses.[3] (c) γ_r and γ_{nr} versus distance for the fluorophores used in the study.

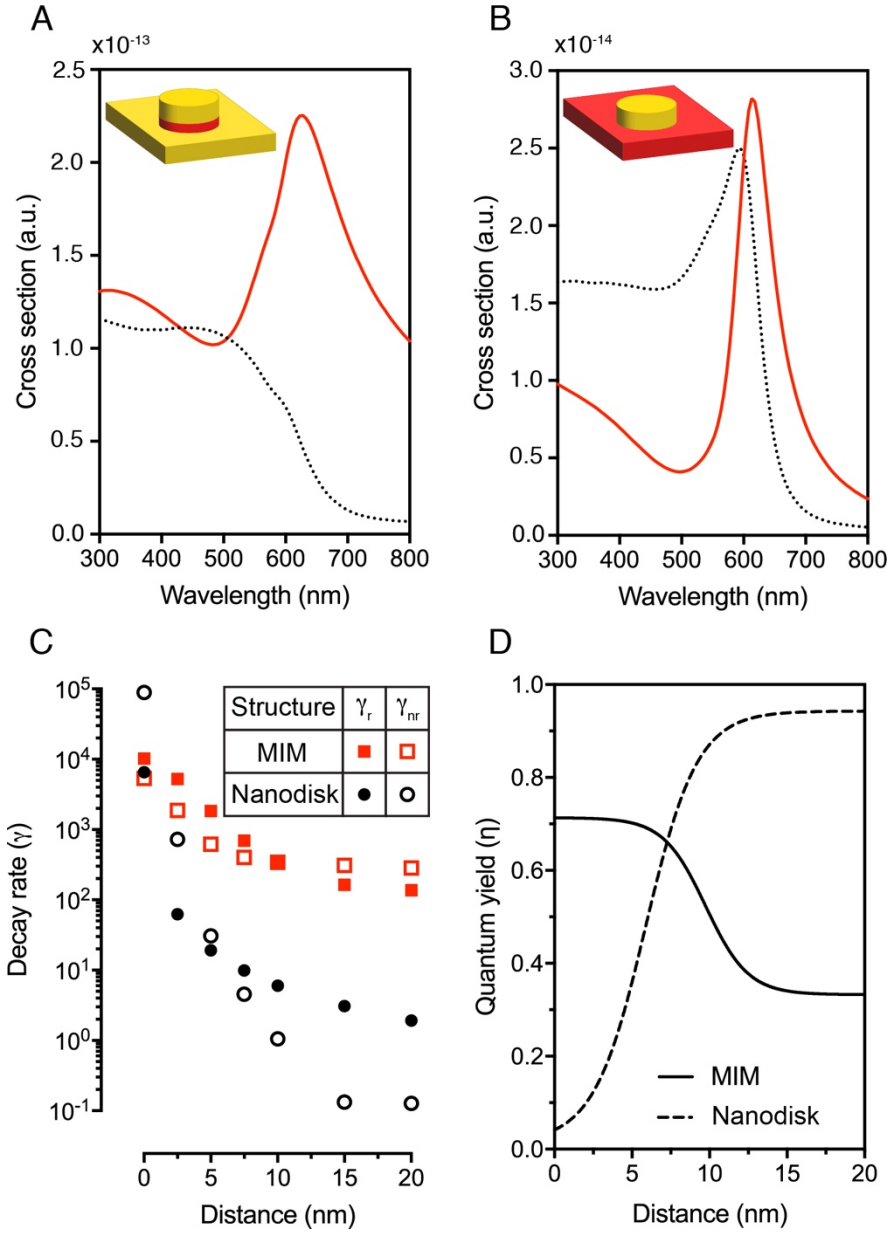

Fig. S5. The absorption (dotted black) and scattering (solid red) cross sections of (a) a 340 nm MIM structure and (b) a 100 nm nanodisk with a matching plasmon resonance computed through FDTD. The resonance of the nanodisk is considerably narrower. (c) The γ_{r} and γ_{nr} for the MIM structure and nanodisk at various distances computed through FDTD. In most cases, the γ_{r} for the MIM structure is orders of magnitude greater than the nanodisk. (d) The structurally-induced quantum yield η for a emitter with an intrinsic quantum yield of unity (η_o = 1) for various distances computed through FDTD. The nanodisk quenches the emitter for distances < 10 nm while the MIM structure suppresses quenching.

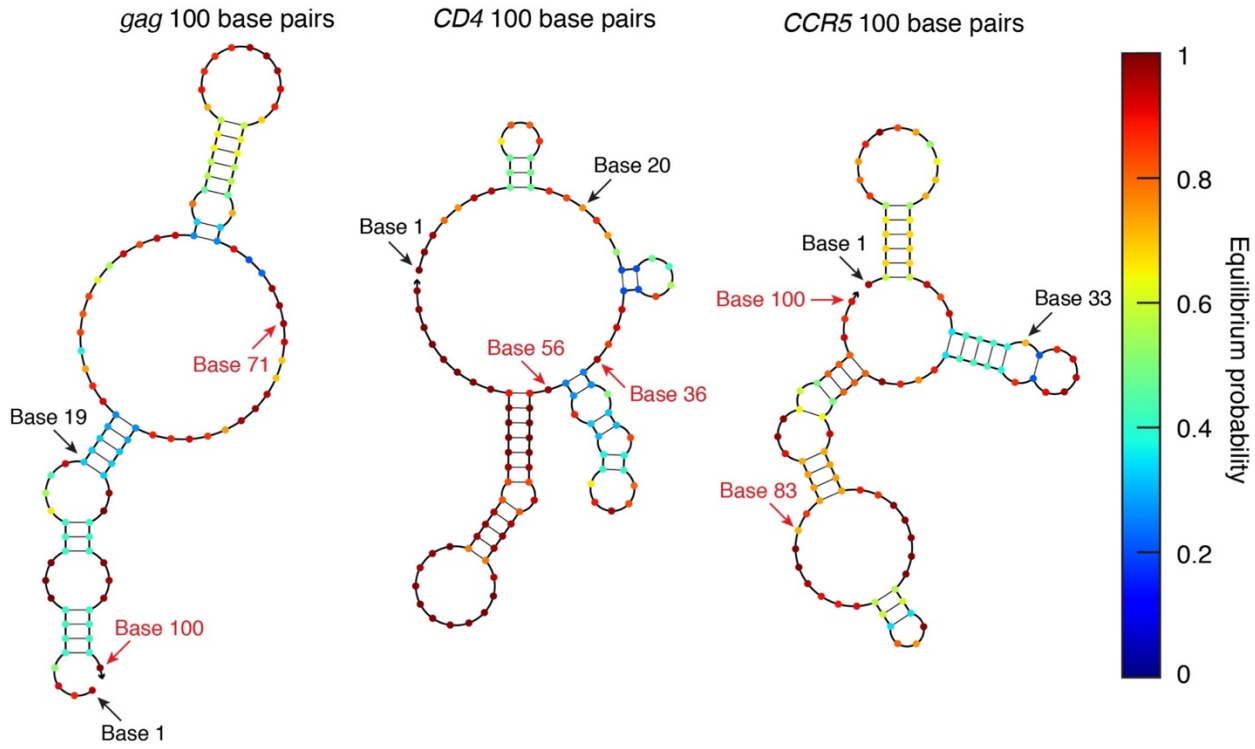

Fig. S6. The design of capture and detection hybridization oligonucleotides using NUPACK.[4] The base sequence range indicated in black (*gag*: bases 1 – 19, *CD4*: bases 1 – 20 and *CCR5*: bases 1 – 33) and red (*gag*: bases 71 – 100, *CD4*: bases 36 – 56 and *CCR5*: bases 83 – 100) correspond to the location of binding of the capture and detection oligos respectively. Regions with a high probability of secondary structure formation were avoided.

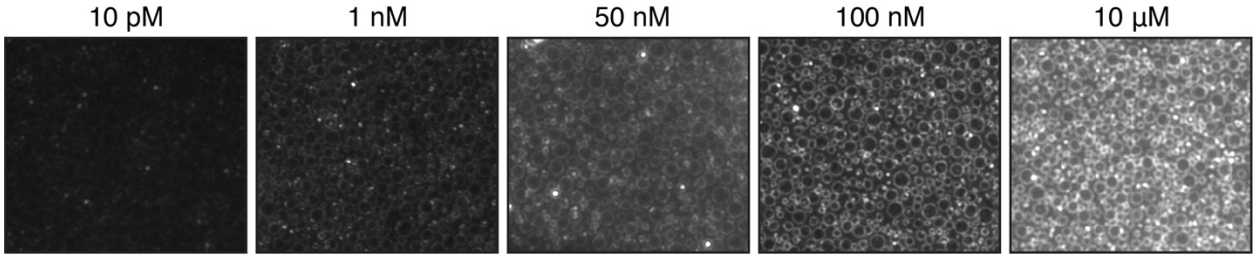

Fig. S7. Fluorescence micrographs of 100-bp CD4 sequence captured and detected from a concentration of 10 pM to 10 µM.

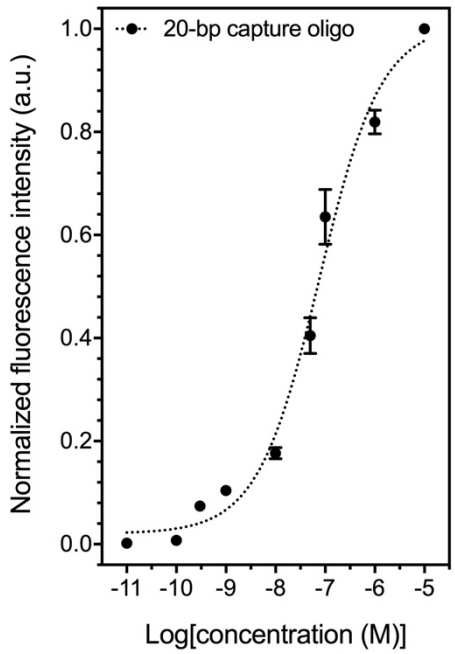

Fig. S8. Normalized fluorescence intensity for the 20-bp *CD4* capture oligo conjugated with AF647. The biosensing of such a small sequence is enabled by the supression of quenching by the quadrupolar mode of the MIM-MS.

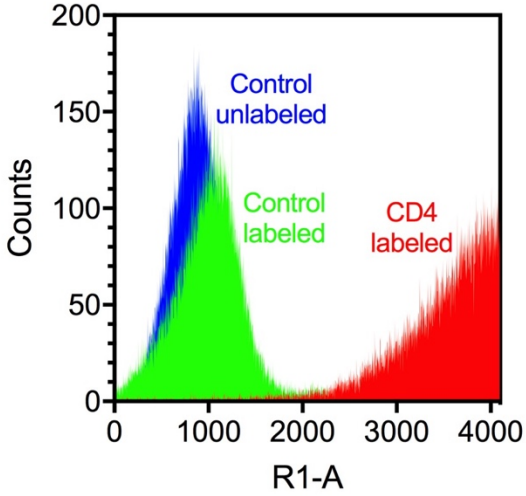

Fig. S9. Flow cytometry histogram indicating high expression of CD4 glycoprotein on the surface of transfected Expi293 cells (red) in comparison to untransfected but labeled Expi293 cells (green) and untransfected unlabeled Expi293 cells (blue).

References

1 C. Huang, Ph.D. Thesis, Technische Universität, 2015.

2 A. K. Kenworthy, K. Hristova, D. Needham and T. J. McIntosh, *Biophysical Journal*, 1995, **68**, 1921–1936.

3 P. B. Johnson and R. W. Christy, *Phys. Rev. B*, 1972, **6**, 4370–4379.

4 J. N. Zadeh, C. D. Steenberg, J. S. Bois, B. R. Wolfe, M. B. Pierce, A. R. Khan, R. M. Dirks and N. A. Pierce, *Journal of Computational Chemistry*, 2011, **32**, 170–173.